IEEE Photonics Journal
An IEEE Photonics Society Publication

Open Access

Investigation and System Implementation of Flexible Bandwidth Switching for a Software-Defined Space Information Network

Volume 9, Number 3, June 2017

Bin Wu
Hongxi Yin
Anliang Liu
Chang Liu
Fangyuan Xing

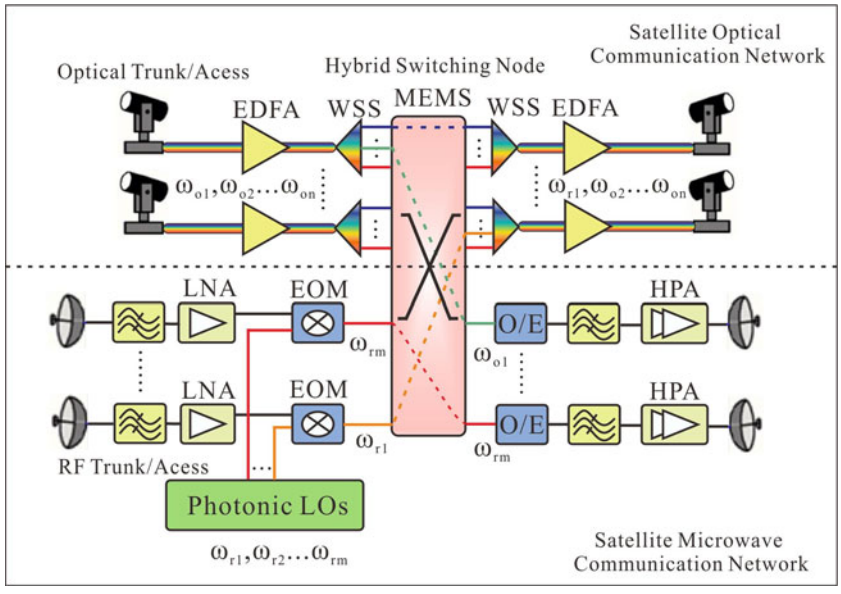

DOI: 10.1109/JPHOT.2017.2705134
1943-0655

Investigation and System Implementation of Flexible Bandwidth Switching for a Software-Defined Space Information Network

Bin Wu, Hongxi Yin, Anliang Liu, Chang Liu, and Fangyuan Xing

Laboratory of Optical Communications and Photonic Technology, School of Information and Communication Engineering, Dalian University of Technology, Dalian 116023, China

DOI:10.1109/JPHOT.2017.2705134

Manuscript received April 20, 2017; revised May 10, 2017; accepted May 12, 2017. Date of publication May 19, 2017; date of current version May 29, 2017. This work was supported in part by the National Natural Science Foundation of China under Grant 61071123 and in part by the Advanced Research Fund of General Armament Department under Grant 113030204-2. Corresponding author: H. Yin (e-mail: hxyin@dlut.edu.cn).

Abstract: This paper proposes and experimentally demonstrates a hybrid switching system that provides flexible bandwidth allocation for future laser and microwave space information networks. First, a switching node structure is designed for laser and microwave hybrid links, and an optimized strategy of flexible bandwidth allocation is presented based on the traffic distribution. Then, we establish a reconfigurable light and microwave hybrid switching system based on microwave photonics. The experimental results indicate that the proposed system can realize microwave frequency conversion and photoelectric hybrid switching. Additionally, bandwidth resources can be allocated flexibly and the bit-error rate of the baseband data is less than 10^{-9}. Furthermore, the simulation results of the proposed flexible bandwidth allocation strategy reveal that the spectrum utilization rate is more than 94% when the traffic is saturated.

Index Terms: Space information networks, light and microwave hybrid switching, microwave photonics, flexible bandwidth.

1. Introduction

With increasing demand from civil and military businesses for high-speed data communication, navigation and positioning, remote sensing and telemetry and high-resolution image acquisition, a higher quality of inter-satellite information transmission, heterogeneous network interconnection and data exchange between multiple types of links is required. Current satellite communications largely depend on microwave transmission and multi-beam switching, and inter-satellite microwave communication has many disadvantages, such as low bandwidth, poor security, severe electromagnetic interference (EMI), large antenna size and high power consumption. This technology will not be able to support the future transmission, switching and rapid processing of high-rate business data [1]. Inter-satellite laser communication has the inherent benefits of high bandwidth, strong security, anti-EMI, small antenna size and low power consumption, which enable highly efficient transmission, exchange and access flexibility for multi-service capacity with multiple granularities [2]. Future space information networks with high bandwidth and flexibility will be heterogeneous hybrid networks, where laser-links and microwave-links coexist and provide complementary

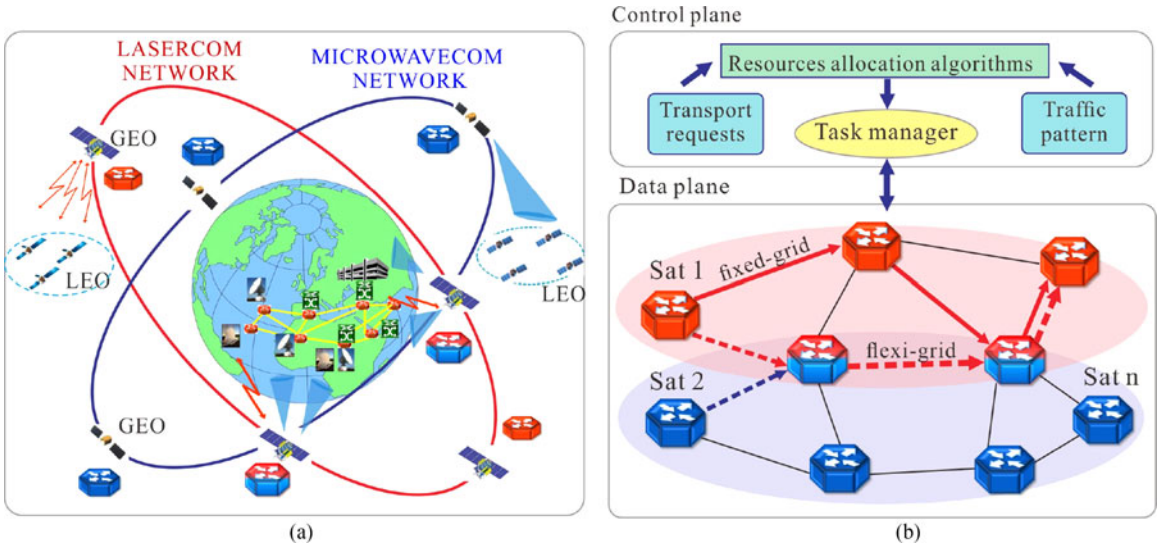

Fig. 1. Laser and microwave hybrid space information networks. (a) Network topology. (b) Functional architecture.

advantages. Therefore, efficient switching and dynamic bandwidth configuration are two of the key technologies to implement space information networks.

Several schemes of bandwidth resources allocation in broadband satellite networks have been reported in the literature. Laser inter-satellite links (ISLs) over the non-geosynchronous satellite constellations based on wavelength division multiplexing (WDM) was proposed in [3]. The wavelength-routed model and wavelength requirements under the time-variant optical ISL topology in WDM optical satellite networks were analyzed in [4] and [5], and the limitations in designing multi-hop ISLs of satellite networks were described in [6]. Using multiple photonic local oscillators (LOs) based on WDM technology, the SAT'N LIGHT project of the European Space Agency (ESA) realized the frequency down conversion of microwave signals [7], [8]. However, the capabilities of light and microwave hybrid switching and flexible bandwidth allocation were not achieved in these research projects.

Current studies of broadband satellite networks generally adopt the method of WDM technology and wavelength allocation to improve the transmission capacity and onboard processing capacity of inter-satellite laser links [9], [10]. To our knowledge, research on light and microwave hybrid switching and flexible bandwidth allocation onboard has not been reported.

Therefore, a flexible bandwidth hybrid switching system that provides flexible bandwidth allocation is developed in this paper. The structure of the switching node is designed, and the optimized allocation strategy with flexible bandwidth is presented based on the traffic distribution. Then, we conduct simulations to compare the advantages and disadvantages of three spectrum resource allocation schemes. A switching system that can achieve the frequency conversion of the microwave link and 10 Gbps single-wavelength data transmission for a laser link is designed and experimentally implemented. Furthermore, the bandwidth resource can be configured flexibly. The experimental results verify the switching capacity of the proposed hybrid node and the feasibility to connect the satellite laser networks with microwave networks.

2. Structure of Space Information Networks and Strategy of Flexible Bandwidth Allocation

2.1 Topology and Architecture of Space Information Networks

The topology and functional architecture of laser and microwave hybrid space information networks are shown in Fig. 1(a) and (b). Satellite laser networks are colored red and satellite microwave

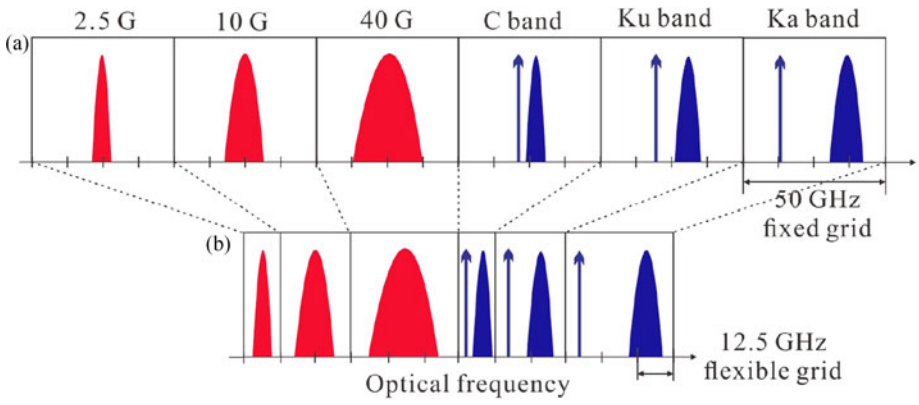

Fig. 2. Comparison diagram of spectrum allocation in space information networks. (a) Traditional WDM optical satellite networks. (b) Flexible bandwidth optical satellite networks.

networks are colored blue in Fig. 1(a); these networks are switched and interconnected by the hybrid switching nodes. Geostationary Earth orbit (GEO) satellites communicate with GEO satellites, low Earth orbit (LEO) satellites, ground stations or terrestrial networks using either laser or microwave links. Moreover, pure optical switching nodes and pure microwave switching nodes are a simplified version of the hybrid nodes. Therefore, the performance of the hybrid switching nodes plays an indispensable role in the networks. The red nodes in Fig. 1(b) are all-optical switching nodes using a fixed grid or flexible grid mode, in accordance with ITU-T standard grids [11]. The blue nodes are all-microwave switching nodes whose microwave bands include the C-band, Ku-band, and Ka-band, among others. Additionally, the red and blue mixed nodes represent light and microwave hybrid switching nodes with service scheduling and spectrum reconfiguration, whose bandwidth allocation uses a flexible grid mode with a minimum bandwidth of 12.5 GHz. The space information networks, composed of these three types of switching nodes, can achieve wavelength-granularity switching in traditional fixed-grid WDM networks and provide sub-wavelength or ultra-long-wavelength flexible bandwidth. Therefore, these networks can meet the future needs of satellite data transmission with multi-bandwidth granularity (including big data in the space data centers).

Based on the transport requests and the onboard traffic pattern, the control plane uses an appropriate resource allocation algorithm and flexible bandwidth partition strategy to re-integrate and allocate the bandwidth resources by controlling the software-defined reconfigurable nodes in the data plane. In addition, according to the different switching granularities of the nodes, the corresponding resource reservation strategy is adopted to reconstruct the spectrum.

Relative to WDM optical satellite networks using a fixed grid mode, the flexible bandwidth space information networks can allocate available frequency resources to the end-to-end optical path by dynamic configuration according to the traffic load and the needs of users. The differences of spectrum allocation between the traditional WDM and the proposed flexible bandwidth optical satellite networks are shown in Fig. 2. A bandwidth of 300 GHz is required to support the services in the traditional manner, while only 150 GHz is required when using flexible bandwidth allocation. Thus, relative to the traditional approach, flexible bandwidth allocation can support fine-grid spectrum segmentation and improve the spectrum utilization.

2.2 Strategy of Flexible Bandwidth Allocation

Flexible bandwidth networks should follow not only spectrum continuity (or wavelength continuity) constraints in traditional WDM optical networks [12]–[14] but also spectrum contiguity constraints. Thus, the frequency resources assigned to each service request must be a contiguous slot. Under the framework of the proposed flexible bandwidth satellite networks, the bandwidth resources onboard are involved in the process of dynamic allocation and release, which leads to time randomness of different granularity traffic [15], [16]. The allocation strategy of traditional satellite networks

will result in a discrete distribution of the idle spectrum. To solve this problem, we propose a strategy of optimized frequency allocation based on the traffic distribution.

Assume that the bandwidths of m sub frequency slots (FS) are SA_1, $SA_2, \ldots, SA_i, \ldots,$ and SA_m after the frequency resources onboard are allocated. Then, we suppose that N requests are necessary to reconstruct spectrum ($R_1, R_2, \ldots, R_j, \ldots, R_N$), the corresponding bandwidth of which is ($B_1, B_2, \ldots, B_j, \ldots, B_N$). The start time point and end time point of each request are st_j and et_j, respectively, and the requests of different rates can only be assigned to their exclusive spectrum area. After the allocation is completed, the maximum sub-FS width occupied in each SA is (S_1, $S_2, \ldots, S_j, \ldots, S_m$). Since we presume $0 < B_j < SA_i$, $j = 1, 2, \ldots, N$, the number m of the divided sub FSs does not exceed N.

$$\text{Set } y_i = \begin{cases} 1 & \text{the requests are assigned to } SA_i \\ 0 & \text{otherwise} \end{cases} \qquad i = 1, 2, \ldots, N \tag{1}$$

$$x_{ij} = \begin{cases} 1 & \text{request } R_j \text{ is reconstructed to } SA_i \\ 0 & \text{reconstruction failure of request } R_j \end{cases} \qquad i, j = 1, 2, \ldots, N \tag{2}$$

The purpose of flexible bandwidth allocation is to accommodate all onboard requests with the least frequency resources. Thus, we use spectrum utilization (SU) as an important index to evaluate the performance of bandwidth allocation strategies; the SU is defined as follows:

$$SU = \sum_{j=1}^{N} B_j x_{ij} / \sum_{i=1}^{N} S_i \tag{3}$$

The linear programming model of the flexible allocation problem is represented as follows:

$$\text{minimize} \quad \sum_{i=1}^{N} y_i S_i \tag{4}$$

$$\text{subjectto} \sum_{j=1}^{N} B_j x_{ij} \leq SA_i \quad i = 1, 2, \ldots, N \tag{5}$$

$$\sum_{i=1}^{N} x_{ij} \leq 1 \tag{6}$$

$$st_j \geq TW_{sj}, \quad et_j \leq TW_{ej} \quad j = 1, 2, \ldots, N \tag{7}$$

The constraint condition (5) indicates that the sum of the request bandwidth allocated to the SA_i cannot exceed the maximum bandwidth of this area. Each request can only be assigned once if it is not blocked, which is represented in constraint condition (6). Additionally, since the time window between the relay satellite and the user satellite is limited after the traffic is generated, each request must be allocated within the corresponding time window [TW_{sj}, TW_{ej}]. Otherwise, the allocation fails, and the request is blocked, which can be found in the constraint condition (7).

2.3 Spectrum Utilization and Network Blocking Probability

A multi-hop optical add-drop network with high-frequency granular optical channel defragmentation was experimentally demonstrated in [17]. Instead of rerouting the traffic of the networks, it only shifts the frequency spectrum to complete the process of reconstruction at the optical add-drop multiplexing (OADM) nodes. Based on this method, we propose two FS allocation strategies, which are shown in Fig. 3(b) and (c), and we have conducted the associated simulations. To compare the performances of the strategies, three spectrum partition methods are evaluated, including the traditional mode and the proposed modes.

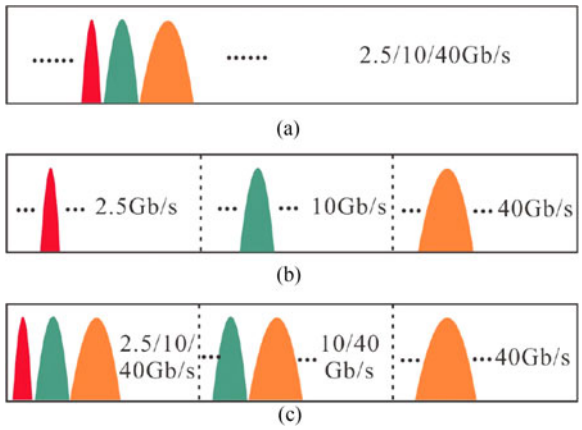

Fig. 3. Three FS allocation strategies. (a) CS, (b) PP, (c) SP.

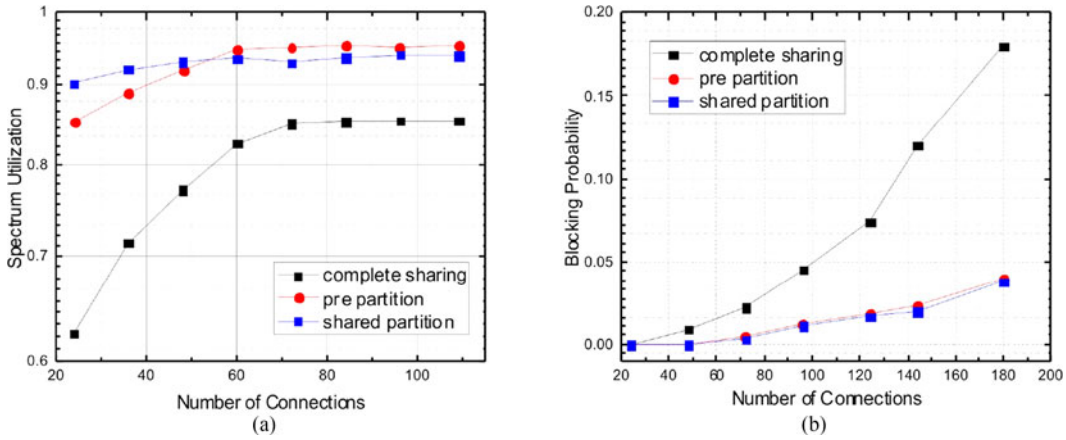

Fig. 4. Comparison of network performance under different spectrum allocation. (a) Spectrum utilization. (b) Blocking probability.

For the traditional complete sharing (CS) mode shown in Fig. 3(a), all rate service requests share the spectrum resources distinguishably. When a new request arrives at the satellite, the lowest-indexed contiguous spectrum that can accommodate the service is selected. The corresponding bandwidth is allocated with the first-fit scheme. Fig. 3(b) is the proposed pre-partition (PP) mode, which partitions the spectrum for dedicated use according to the distribution of different bandwidth connections. Each partition of the spectrum carries the same bandwidth requests and resources can be allocated using any existing wavelength assignment and routing schemes within each partition. The reasonable spectrum partition scheme is adopted to avoid the traffic congestion caused by the non-contiguous spectrum resulting from high-bandwidth requests. Vertical fragmentation caused by unfair contentions of different bandwidths can be eliminated. To exploit both sharing and partition, the shared-partition (SP) mode is proposed as shown in Fig. 3(c). SP mode is a hybrid scheme which can achieve a fine balance of partitioning and sharing to increase the spectrum allocation efficiency. Higher-rate requests are allocated larger shares of the spectrum resources, because they are more likely to be blocked by the lower-rate requests.

Assuming that the requests of various rates have the same traffic intensity, the accessing requests for 2.5 Gbps, 10 Gbps, 40 Gbps and 100 Gbps rates are assigned 1, 2, 3 and 8 FSs, respectively. We compare the SU and blocking probability of both the traditional CS mode and the proposed PP and SP modes, and the simulation results are shown in Fig. 4(a) and (b).

As illustrated in Fig. 4(a), the SU of the three FS allocation strategies increase with the rising number of connection requests and tend to be stable when the number of connections is greater

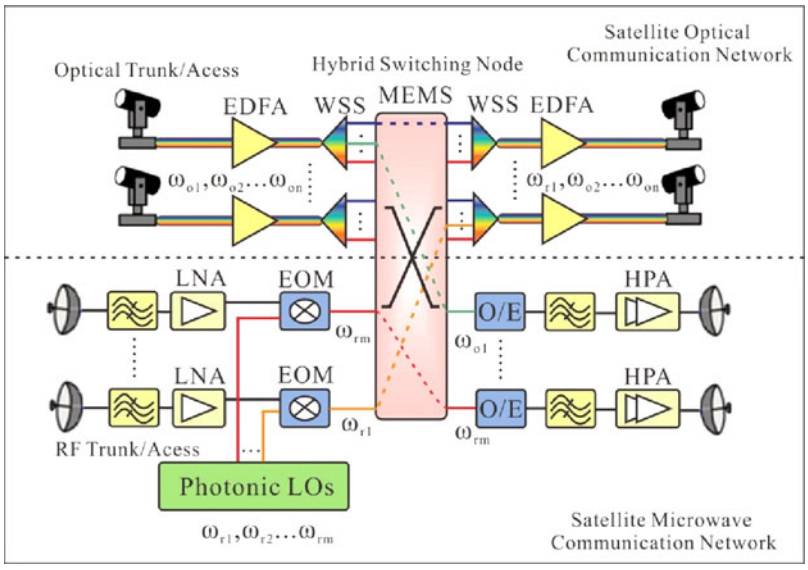

Fig. 5. Schematic diagram of laser and microwave link hybrid switching node.

than 70. If there are the same number of connection requests, the SU of PP and SP is higher than that of the traditional CS mode. PP and SP can be as high as 94% when the network is highly loaded, while CS causes a nearly 15% loss of spectrum resources due to spectrum fragmentation. When the traffic load is low, the SU of PP mode is inferior to that of the SP mode on account of the cost of spectrum partitioning, but it surpasses that of the SP mode when the number of connections is greater than 60. Nevertheless, the SP mode is relatively straightforward to implement and flexible in practice since each rate of request occupies the spectrum in the sharing manner. The results illustrate the trade-off of spectrum sharing versus partitioning. When the network experiences very low blocking, it is more efficient to encourage spectrum sharing, while when the network is highly loaded, more partitioning would avoid the conflicts between lower-bandwidth and higher-bandwidth requests, which can increase the spectrum utilization effectively. Fig. 4(b) shows that the blocking probability of SP and PP increases moderately with the increase of node traffic, yet the blocking probability of CS increases notably. This result suggests that adopting CS mode to allocate the frequency will cause high-rate accessing requests to be blocked by discrete low-rate ones, resulting in additional spectrum fragmentation and eventually leading to a high probability of blocking. Therefore, the proposed PP and SP spectrum allocation strategies retain a relatively high SU and effectively reduce the network blocking probability.

3. Structure and Principle of Hybrid Switching Node with Laser and Microwave Links

3.1 Structure of Hybrid Switching Node

Based on the proposed space information network architecture of flexible bandwidth switching, a hybrid switching node with laser and microwave links is designed. The schematic diagram is shown in Fig. 5. The upper part of the node implements the switching between the channels of the laser links, which are composed of an Erbium-doped fiber amplifier (EDFA), wavelength selective switches (WSS) [18], [19] and a microelectromechanical system (MEMS) optical switching array [20], [21]. It is a circuit switch that reconstructs the spectrum, allocates and configures the bandwidth dynamically before the data reaches the node using the control of the signaling and protocol from signaling networks, and then builds the links to complete the switching. After the switching process is finished, the links are broken to release spectrum resources for the next switching request under the control of the signaling networks.

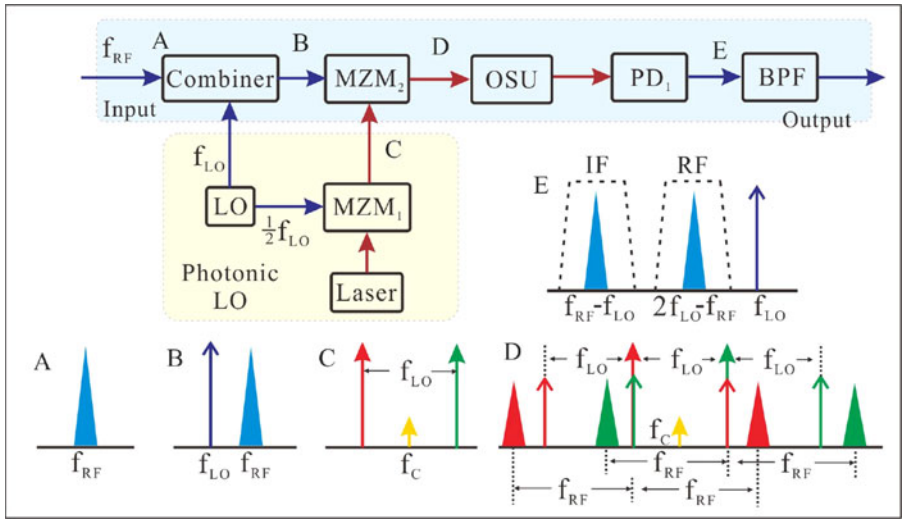

Fig. 6. Structure and principle of RF conversion node based on microwave photonics.

The lower part of the node realizes the switching between the channels of the microwave links and the conversion of the microwave frequency in the optical domain. Based on microwave photonics techniques, the microwave signals of different bands are filtered and amplified by a low-noise amplifier (LNA) and subsequently mixed with a multi-frequency optical LO in the optical domain through an electro-optical modulator (EOM). Following that process, the optical signal is switched to the corresponding channel by MEMS. After the beating through the photodetector, the target frequency components are filtered out. The radio frequency (RF) is eventually converted to another RF or intermediate frequency (IF) that matches the frequency band of the destination node to implement the switching and accessing of the microwave links. Since this part employs an optical processing method to achieve the switching of microwave links, it greatly improves the switching performance and has the advantages of high bandwidth, low loss, low crosstalk, small size, low power consumption and simple implementation. Furthermore, this part also performs the function of frequency conversion, which significantly reduces the resource conflicts of the export, decreases the blocking probability of switching and accessing and improves the utilization of spectrum resources.

Moreover, the light and microwave hybrid switching node also performs the electrical-optical and optical-electrical switching function, which can either switch the microwave accessing signal from the LEO and ground station to the optical domain or convert the data from the laser links of satellite backbone networks to the microwave domain. This process achieves high-performance, flexible and efficient switching and accessing; therefore, pure microwave switching nodes in microwave satellite networks and pure optical switching nodes in optical satellite networks should be special types of our proposed hybrid switching node, which has the same function as its subset and will not be described again in detail.

3.2 Principle of Frequency Conversion

Compared to traditional microwave switching, the light and microwave hybrid switching nodes based on microwave photonics can support higher frequency bands and provide additional processing capacity, making cross-connections between channels and frequency conversion more flexible [22], [23]. The structure and conversion principle of the proposed frequency conversion node are illustrated in Fig. 6.

Among several microwave channels in the lower part of the node, we assume that the center frequency of the input RF signal from a certain channel is f_{RF}, as shown in point A of Fig. 6. Then, the RF signal is combined with the single-tone signal from LO, whose frequency is f_{LO}. The output

signal of the combiner, whose spectrum shown in point B of Fig. 6, is sent to the Mach-Zehnder modulator (MZM) for mixing.

The photonic LO is generated by double-sideband suppressed-carrier (DSB-SC) modulation, with the MZM_1 biased at the minimum transmission point (MITP) of the modulation curve. The electrical LO frequency of the MZM_1 input signal is $0.5f_{LO}$. The spectrum of photonic LO out of MZM_1 is shown in point C, and its electrical field can be expressed as

$$E_c(t) = E_{in}(t)\cos\left(\frac{\pi V_{bias}}{2V_\pi} + \frac{\pi V_{LO}(t)}{2V_\pi}\right) \tag{8}$$

where $E_{in}(t) = \sqrt{2P_{in}}e^{j\omega_c t}$ is the electrical field of the optical carrier, P_{in} is the output optical power of the laser, and ω_c is the angular frequency of the optical carrier. The bias voltage of MZM_1 is $V_{bias} = V_\pi + 2mV_\pi$ (where m is an integer), while the modulating voltage $V_{LO}(t)$ is applied differentially to the two arms via the voltages $V_1(t)$ and $V_2(t)$. This process is represented by $V_{LO}(t) = V_1(t) - V_2(t) = V_{LO}\cos(\frac{1}{2}\omega_{LO}t)$. V_π is the MZM_1 switching voltage, and V_{LO} is the amplitude of the electrical signal into MZM_1. If the MZM_1 is under the MITP modulation scheme with $m = 0$, the optical signal at point C can be written as

$$\begin{aligned} E_C(t) &= -\sqrt{2P_{in}}e^{j\omega_c t}\sin\left(\frac{\pi V_{LO}}{2V_\pi}\cos\left(\frac{1}{2}\omega_{LO}t\right)\right) \\ &= \sqrt{2P_{in}}e^{j\omega_c t}\left[2\sum_{n=1}^{\infty}(-1)^n J_{2n-1}(\beta_1)\cos\left(\frac{(2n-1)}{2}\omega_{LO}t\right)\right], n = 1, 2, \ldots \end{aligned} \tag{9}$$

where $\beta_1 = \frac{\pi V_{LO}}{2V_\pi}$ represents the phase modulation index and $J_{2n-1}(\cdot)$ is the Bessel function of the first kind.

Equation (9) indicates that only odd-order harmonics exist in the optical field and that even-order harmonics and optical carriers are suppressed. When the higher-order sidebands are neglected and the insertion loss of the MZM_1 is assumed to be zero, the output optical signal of the photonic LO can be written as

$$E_C(t) = -\sqrt{2P_{in}}J_1(\beta_1)\left[e^{j\left(\omega_c+\frac{1}{2}\omega_{LO}\right)t} + e^{j\left(\omega_c-\frac{1}{2}\omega_{LO}\right)t}\right] \tag{10}$$

Therefore, the two sideband frequencies of photonic LO signals with carrier suppression are $\omega_c + \frac{1}{2}\omega_{LO}$ and $\omega_c - \frac{1}{2}\omega_{LO}$. Subsequently, the signal of the photonic LO is mixed with the output signal of the combiner by MZM_2 in the frequency domain, the output spectrum of which is shown in point D of Fig. 6. When only the upper sideband is assumed as the carrier, the electrical field intensity after mixing can be expressed as the green part of spectrum D.

$$\begin{aligned} E_{D\_USB}(t) = &-\sqrt{P_{in}}J_1(\beta_1)[J_0(\beta_1) + J_0(\beta_2)]e^{j\left(\omega_c+\frac{1}{2}\omega_{LO}\right)t} \\ &+ \sqrt{P_{in}}J_1(\beta_1)J_1(\beta_1)\left[e^{j\left(\omega_c+\frac{3}{2}\omega_{LO}\right)t} + e^{j\left(\omega_c-\frac{1}{2}\omega_{LO}\right)t}\right] \\ &+ \sqrt{P_{in}}J_1(\beta_1)J_1(\beta_2)\left[e^{j\left(\omega_c+\frac{1}{2}\omega_{LO}+\omega_{RF}\right)t} + e^{j\left(\omega_c+\frac{1}{2}\omega_{LO}-\omega_{RF}\right)t}\right] \end{aligned} \tag{11}$$

where $\beta_2 = \frac{\pi V_{RF}}{2V_\pi}$ is the phase modulation index. Similarly, with the lower sideband serving as the carrier, the frequency components are $\omega_c - \omega_{LO}/2$, $\omega_c + \omega_{LO}/2$, $\omega_c - 3\omega_{LO}/2$, $\omega_c - \omega_{LO}/2 + \omega_{RF}$ and $\omega_c - \omega_{LO}/2 - \omega_{RF}$ after mixing (the red part of the spectrum D). The signal passes through the optical switching unit (OSU) into the photodetector for frequency conversion. Two frequency components carrying data are obtained by frequency beating through the photodetector: the IF signal of the center frequency $f_{RF} - f_{LO}$ and the RF signal of the center frequency $2f_{LO} - f_{RF}$. The LO signal of center frequency f_{LO} is outputted as well. The spectrum diagram is shown in point E of Fig. 6.

Finally, after the bandpass filter (BPF) chooses the corresponding frequency components according to the demand, the RF signal is converted to an RF signal ($f_{RFout} = 2f_{LO} - f_{RF}$) or IF signal ($f_{IFout} = f_{RF} - f_{LO}$) to complete the node frequency conversion function.

By changing the frequency of the photonic LO or adopting the tunable photonic LO, the architecture can achieve flexible multi-channel switching between satellite microwave links and frequency conversion, which supports channel switching of the S/C/Ku/Ka band and provides relay services for microwave satellites of different operating frequencies. Additionally, the down-converted IF signal can be transmitted to microwave ground stations through the downlink channels or processed onboard for date recovery, regeneration, storage or other purposes.

4. Experimental Results for the Space Information Network Switching System

4.1 Experiment on the Frequency Conversion of Microwave Links

Based on the proposed laser and microwave switching structure of space information networks, we established an experimental system to verify the switching capacity of the network relay nodes and feasibility of applying the microwave photonic technique to onboard processing. The structure diagram of the microwave link switching and frequency conversion experimental system is shown in Fig. 7(a), and Fig. 7(b) shows a photograph of the test apparatus.

First, based on the circuits we developed, the RF input signal generation unit generates the Ka band signal, the center frequency of which is 28 GHz, as an input signal of the back-end switching unit. The BERT (Anritsu MP1800A) generates 100 Mbps and 500 Mbps baseband data with the pattern of 2^7-1 and $2^{31}-1$ PRBS. The microwave signal is generated by two up-conversion cycles, and the baseband data are mixed with the 2 GHz and 26 GHz LO signal, to obtain a DSB modulated signal with 26 GHz carrier (point A in Fig. 7). The center frequency of the upper sideband and the lower sideband are 28 GHz and 24 GHz, respectively; the spectrum of 26 GHz carrier and the upper sideband signal are filtered out by an amplifier and a BPF, which is measured by the spectrum analyzer (Rohde & Schwarz FSVR40) as shown in Fig. 8.

Subsequently, the photonic multi-LO generation unit outputs the photonic LO signal for back-end mixing. The photonic LO signal is generated by an optical double-sideband suppressed-carrier modulated scheme (point C in Fig. 7). We use two electric phase shifter (EPS) circuits to adjust the phase in each arm of MZM_1. The phase offsets of the two EPS circuits are set as 0° and 180°. The insertion losses of the two EPS circuits are the same and the voltages of the MZM_1 input signals are equal and opposite, which is referred to as the push-pull mode. Therefore, the EPS circuits will not break the balance between the arms and work in a chirp-free mode. The frequency of the LO signal into the dual-drive MZM_1 is 13 GHz, and the DC bias voltage is set to V_π. The center frequency difference of the MZM_1 output signal between the first order upper sideband and the lower sideband is 26 GHz, and the output spectrum of the MZM_1 as measured by an optical spectrum analyzer (Anritsu MS9740A) is shown in Fig. 9(a).

Afterwards, the microwave photonic switching and processing unit realizes the channel switching and frequency conversion function. The 28 GHz electrical signal from the RF signal generation unit and the optical signal from the photonic LO are mixed by a 40 GHz bandwidth MZM_2 (Photline MX-LN-40). The spectrum of the output optical signal (point D in Fig. 7) is shown in Fig. 9(b). The wavelengths corresponding to the four peaks in Fig. 9(b) are 1549.244 nm, 1549.468 nm, 1549.676 nm and 1549.900 nm. The corresponding frequency differences are 27.97 GHz, 25.97 GHz and 27.97 GHz, which are consistent with our theoretical analysis.

The mixed optical signal is processed by the EDFA and the variable optical attenuator (VOA) and then reaches the all-optical switching unit composed of an 8×8 optical switching matrix based on MEMS optical switches. After the computer-controlled switching is completed, the optical signal reaches the 40 GHz bandwidth photodetector (Finisar XPDV2120) for beat frequency analysis. The frequency of the output electrical signal includes an IF component of $28 - 26 = 2$ GHz and an RF component of $2 \times 26 - 28 = 24$ GHz (point E in Fig. 7). Ultimately, we obtain the IF/RF signal passed through the BPF; the spectra measured by a spectrum analyzer (Keysight N9020A) are shown in Fig. 10(a) and (b).

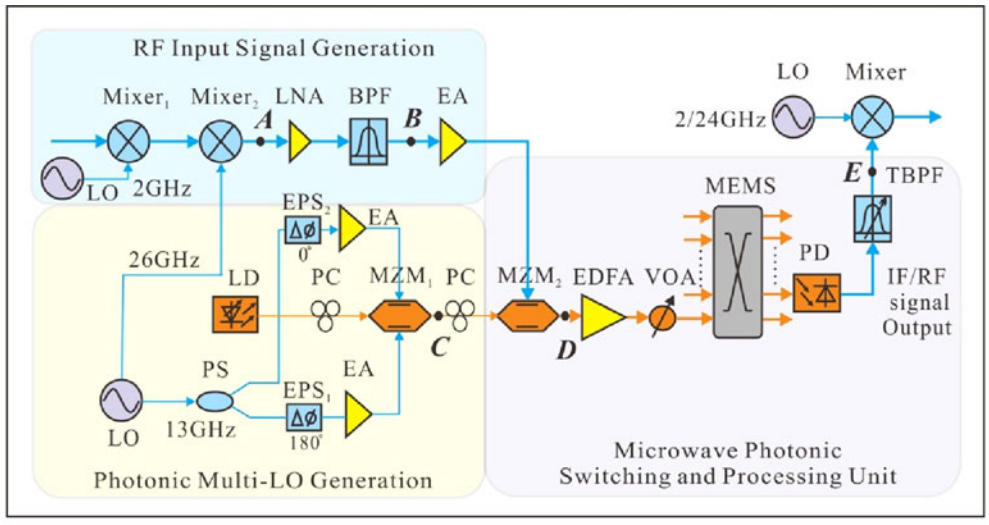

(a)

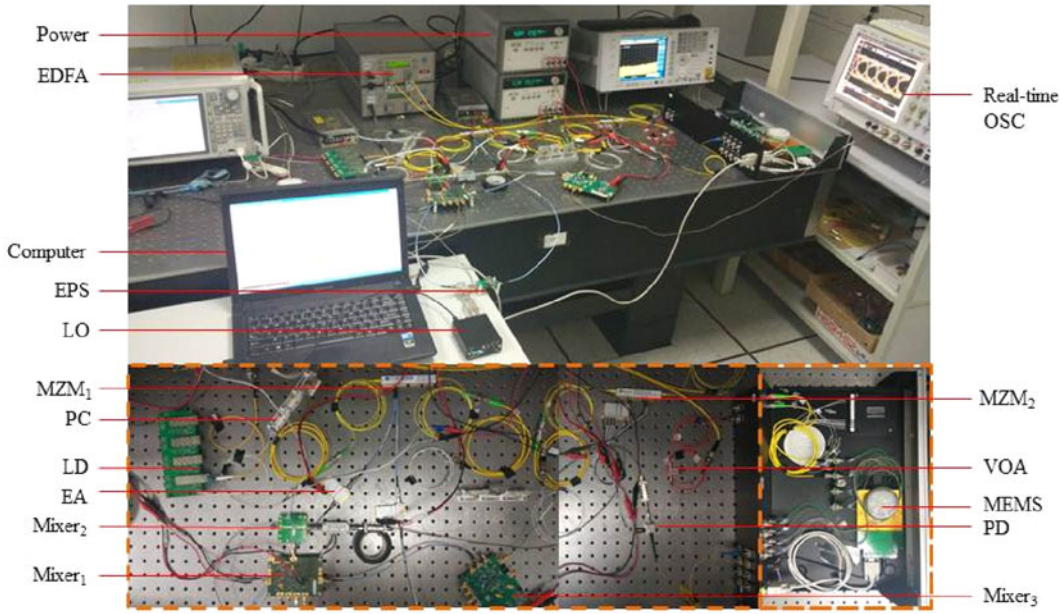

(b)

Fig. 7. Structural diagram and photograph of the microwave link switching and frequency conversion experiment. (a) Structural diagram of the experimental system. (b) Identification experiment. LNA: low-noise amplifier, BPF: bandpass filter, EA: electric amplifier, LD: laser diode, PC: polarization controller, MZM: Mach-Zehnder modulator, PS: power splitter, EPS: electric phase shifter, EDFA: Erbium-doped fiber amplifier, VOA: variable optical attenuator, MEMS: microelectromechanical system, PD: photodiode, TBPF: tunable bandpass filter, OSC: oscilloscope.

To simulate receiving data from target satellites or ground station and verifying the signal quality, the LO is used for demodulation, and the original baseband data after low-pass filtering is obtained. Fig. 11 shows the eye diagrams of the baseband data, the data rates of which are 100 Mbps and 500 Mbps with test pattern lengths of 2^7-1 and $2^{31}-1$. The bit-error rate (BER) as measured by the Anritsu MS9740A is less than 10^{-9}.

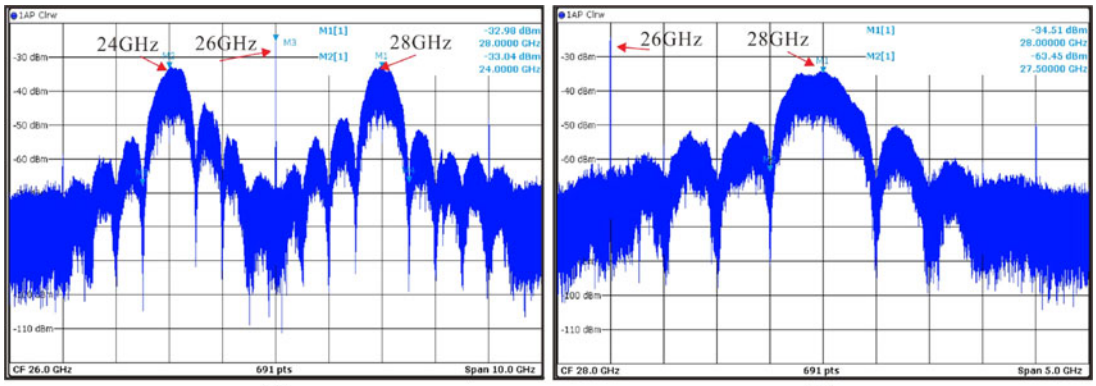

Fig. 8. Spectra of 28 GHz RF input signal. (a) Double-sideband signal. (b) Output signal of the filter.

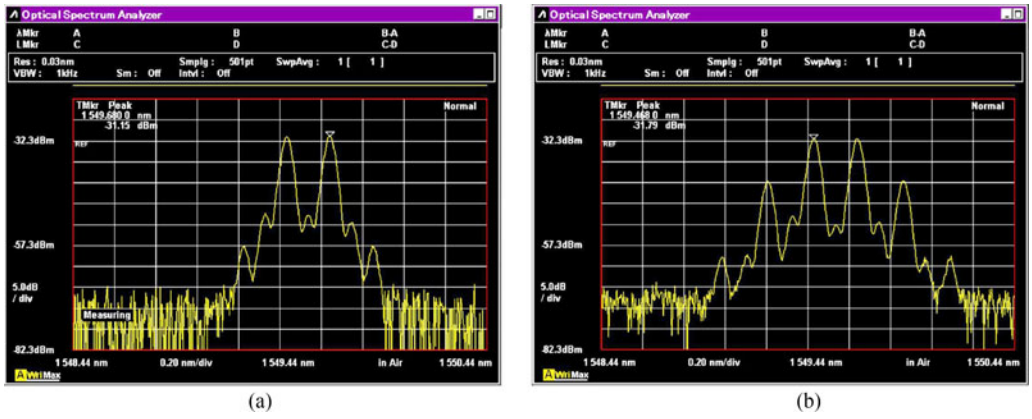

Fig. 9. Spectra of the output optical signal. (a) Optical LO signal. (b) Output signal of MZM after mixing.

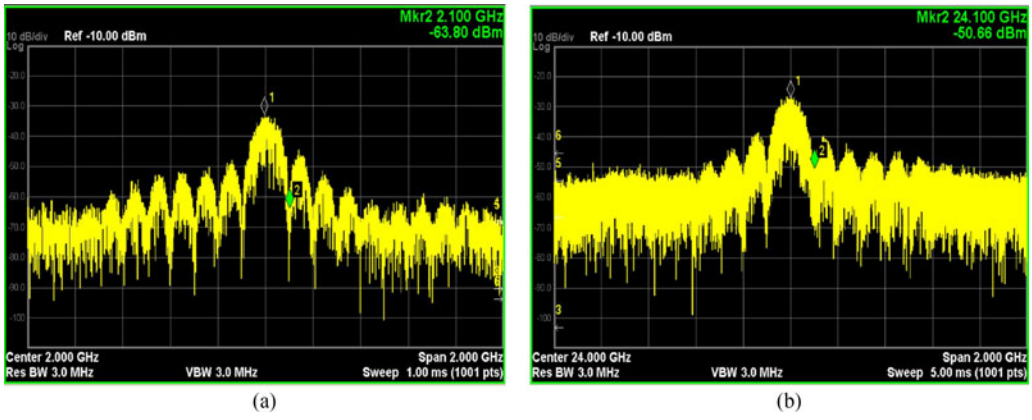

Fig. 10. Spectra of the electrical signal after frequency conversion. (a) 2 GHz IF signal. (b) 24 GHz RF signal.

4.2 Experiment on the Flexible Bandwidth Allocation of Laser Links

To test the flexible bandwidth switching capacity of the laser links and the influence of the MEMS optical switching unit on the system BER, we constructed an experimental system as shown in Fig. 12.

Primarily, the front-end optical signal generation unit simulates the input signal of the switching unit. The optical signal from the broadband laser source is divided into four channels by a

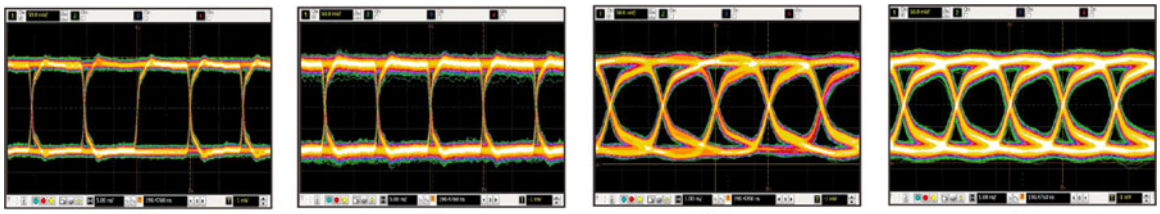

Fig. 11. Eye diagrams of the baseband data. (a) Rate: 100 Mbps, PRBS length: 2^7-1. (b) Rate: 100 Mbps, PRBS length: $2^{31}-1$. (c) Rate: 500 Mbps, PRBS length: 2^7-1. (d) Rate: 500 Mbps, PRBS length: $2^{31}-1$.

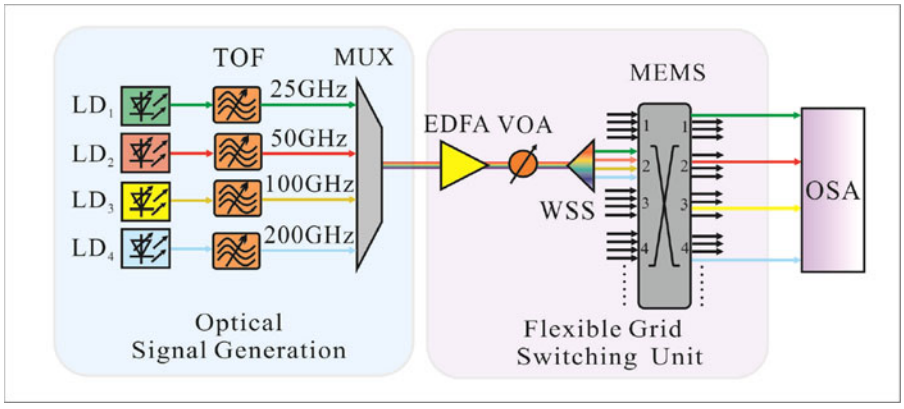

Fig. 12. Structural diagram of the laser-link flexible bandwidth allocation experiment. TOF: tunable optical filter, MUX: multiplexer, WSS: wavelength selective switches, OSA: Optical Spectrum Analyzer.

1:4 optical power splitter and sent to the tunable optical filter (TOF). Its center wavelengths are 1552.37 nm, 1553.98 nm, 1555.19 nm and 1555.89 nm, and the passband widths are 25 GHz, 50 GHz, 100 GHz and 200 GHz. The optical signals of four different bandwidths simulate the services of different rates from the front-end carrier. The signals reach the optical switching unit as the input of optical-link port 2 after being multiplexed by the multiplexer (MUX) and amplified by the EDFA.

Subsequently, the bandwidth is allocated based on the WSS in the switching unit. The channel spacing, center wavelength and attenuation of the WSS are configured by the control command from the controller, and the parameters above are consistent with the TOF. After being switched by MEMS optical switches, four optical signals are sent to output ports 1-4 of the laser links. The spectra of four channels measured by the Anritsu MS9740A are shown in Fig. 13, which verifies that the laser links of the hybrid switching node have the abilities of dynamic bandwidth allocation and elastic bandwidth switching.

Finally, the relationship between the received optical power and the BER and the phase noise performance is tested with or without OSU. The data rate of the tested laser links is 10 Gbps, and the BER experimental results are shown in Fig. 14. The figure shows that the BER gradually increases as the received optical power decreases, and the laser link BER is less than 10^{-9} when the received optical power is greater than -21.6 dBm. Thus, the proposed switching unit does not impact the system BER significantly.

The phase noise performance of the node is also investigated with or without the MEMS switching unit. Fig. 15 shows the relative phase noises of the IF signal. The results show that there is no observable increase in phase noise of microwave signals and the phase noise level is not affected by the MEMS switching unit. Therefore, the switching structure proposed in this study will not degrade phase noise performance of the system.

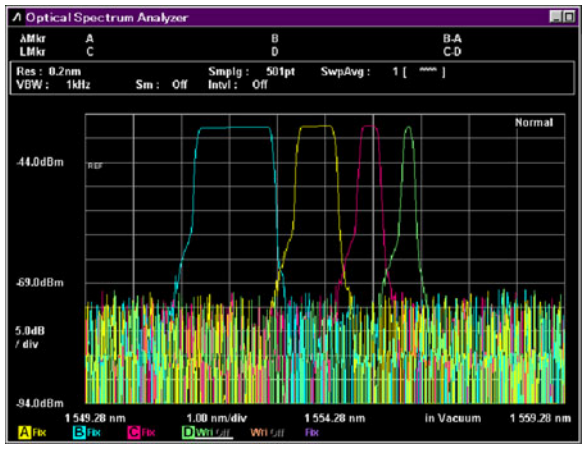

Fig. 13. Spectra of the four channels of the MEMS optical switches.

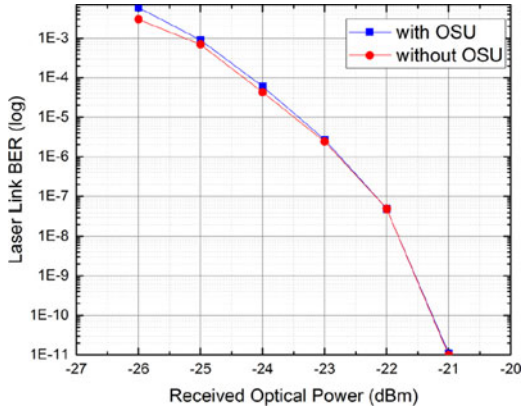

Fig. 14. BER curve of the single-wavelength 10 Gbps data transmission experiment of laser links.

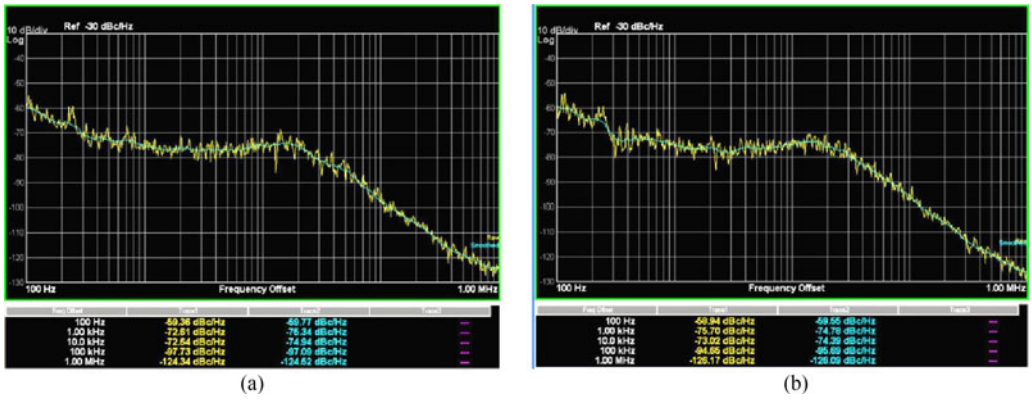

Fig. 15. Phase noise at IF frequency (a) without the MEMS switching unit or (b) with the MEMS switching unit.

5. Conclusion

In this paper, a flexible bandwidth light and microwave hybrid switching system that is applicable to future space information networks is proposed, and the corresponding flexible bandwidth resource allocation strategy is investigated. First, we compare the advantages and disadvantages of the three spectrum resource allocation strategies. The simulation results show that the flexible bandwidth

allocation strategy we propose reduces spectrum resource loss by nearly 15% relative to the traditional CS mode when the traffic is saturated. Then, the structure of the light and microwave hybrid switching node is presented, and the principle and the key technologies of the switching are analyzed. Finally, we develop the circuits and establish an experimental test apparatus to verify the abilities of light and microwave hybrid switching, microwave frequency conversion and flexible bandwidth allocation.

The experimental results indicate that the microwave links of the node can realize all-optical transparent processing of signals through the photoelectric mixer, which can implement the switching and interconnection onboard between the channels of the S/C/Ku/Ka band in the microwave satellite networks. The laser link can transmit 10 Gbps data with a single wavelength, whose baseband data BER is less than 10^{-9}, and the channel bandwidth can be flexibly allocated. The hybrid node designed can converge onboard for laser links and microwave links in future space information networks to provide the benefits of high efficiency and reliability, anti-interference, and flexible applications, among other advantages.

References

[1] M. Toyoshima, "Trends in satellite communications and the role of optical free-space communications," *J. Opt. Netw.*, vol. 4, no. 6, pp. 300–311, Jun. 2005.
[2] J. Yao, "Microwave photonics," *J. Lightw. Technol.*, vol. 27, no. 1-4, pp. 314–355, Jan. 2009.
[3] N. Karafolas and S. Baroni, "Optical satellite networks," *J. Lightw. Technol.*, vol. 18, no. 12, pp. 1792–1806, Dec. 2000.
[4] L. Tan, Q. Yang, and J. Ma, "Wavelength dimensioning of optical transport networks over nongeosychronous satellite constellations," *J. Opt. Commun. Netw.*, vol. 2, no. 4, pp. 166–174, Apr. 2010.
[5] Q. Yang, L. Tan, and J. Ma, "An analytic method of dimensioning required wavelengths for optical WDM satellite networks," *IEEE Commun. Lett.*, vol. 15, no. 2, pp. 247–249, Feb. 2011.
[6] D. Kedar and S. Arnon, "Backscattering-induced crosstalk in WDM optical wireless communication," *J. Lightw. Technol.*, vol. 23, no. 6, pp. 2023–2030, Jun. 2005.
[7] M. Sotom, B. Benazet, A. Le Kernec, and M. Maignan, "Microwave photonic technologies for flexible satellite telecom payloads," in *Proc. 35th Eur. Conf. Opt. Commun.*, Sep. 2009, pp. 1–4.
[8] N. Karafolas, J. Armengol, and I. Mckenzie, "Introducing photonics in spacecraft engineering: ESA's strategic approach," in *Proc. IEEE Aerosp. Conf.*, Mar. 2009, pp. 1–15.
[9] L. Gu, F. Zhao, Z. Shi, J. Liu, and R. Chen, "Four-channel coarse WDM for inter- and intra-satellite optical communications," *Opt. Laser Technol.*, vol. 37, no. 7, pp. 551–554, Oct. 2005.
[10] X. Yang *et al.*, "Optical frequency comb based multi-band microwave frequency conversion for satellite applications," *Opt. Exp.*, vol. 22, no. 1, pp. 869–877, Jun. 2014.
[11] ITU-T Study Group 15, "ITU-T G.694.1: Spectrum grids for WDM applications: DWDM frequency grid, 2012.
[12] Z. Xu *et al.*, "Flexible bandwidth allocation in filterless optical networks," *IEEE Commun. Lett.*, vol. 19, no. 4, pp. 565–568, Apr. 2015.
[13] J. Comellas and G. Junyent, "Improving link spectrum utilization in flexgrid optical networks," *J. Opt. Commun. Netw.*, vol. 7, no. 7, pp. 618–627, Jul. 2015.
[14] M. Shiraiwa, H. Furukawa, T. Miyazawa, Y. Awaji, and N. Wada, "High-speed wavelength resource reconfiguration system concurrently establishing/removing multiwavelength signals," *IEEE Photon. J.*, vol. 8, no. 2, pp. 1–7, Feb. 2016.
[15] T. Foggi, G. Colavolpe, A. Bononi, and P. Serena, "Spectral efficiency optimization in flexi-grid long-haul optical systems," *J. Lightw. Technol.*, vol. 33, no. 13, pp. 2735–2742, Jul. 2015.
[16] M. Hadi and M. Pakravan, "Spectrum-convertible BVWXC placement in OFDM-based elastic optical networks," *IEEE Photon. J.*, vol. 9, no. 1, pp. 1–12, Feb. 2017.
[17] S. Shimizu, G. Cincotti, and N. Wada, "Demonstration of multi-hop optical add-drop network with high frequency granular optical channel defragmentation nodes," in *Proc. Opt. Fiber Commun. Conf. Exhibition*, Mar. 2015, pp. 1–3.
[18] D. Xie *et al.*, "LCoS-based wavelength-selective switch for future finer-grid elastic optical networks capable of all-optical wavelength conversion," *IEEE Photon. J.*, vol. 9, no. 2, pp. 1–12, Apr. 2017.
[19] M. Niwa, Y. Mori, H. Hasegawa, and K. Sato, "Novel optical-node architecture utilizing asymmetric-multiport wavelength-selective switches," *IEEE Photon. J.*, vol. 8, no. 2, pp. 1–10, Apr. 2016.
[20] S. Hernandez, M. Zahir, F. Filhol, and L. Marchand, "MOEMS for space application. The European Space Agency strategy for photonics components," *Proc. SPIE*, vol. 7594, 2010, Art. no. 75940S.
[21] B. Guldimann, L. Venancio, K. Wallace, J. Perdigues, Z. Sodnik, and B. Furch, "Space instruments based on MOEMS technology," in *Proc. IEEE Conf. Opt. MEMs Nanophotonics*, Aug. 2008, pp. 126–127.
[22] W. Li, L. Wang, J. Zheng, M. Li, and N. Zhu, "Photonic MMW-UWB signal generation via DPMZM-based frequency up-conversion," *IEEE Photon. Technol. Lett.*, vol. 25, no. 19, pp. 1875–1878, Oct. 2013.
[23] W. Li and J. Yao, "Investigation of photonically assisted microwave frequency multiplication based on external modulation," *IEEE Trans. Microw. Theory Techn.*, vol. 58, no. 11, pp. 3259–3268, Nov. 2010.